LHCHXSWG-2019-001

March 1, 2019

LHC HIGGS CROSS SECTION WORKING GROUP[1]

PUBLIC NOTE

Higgs boson cross sections for the high-energy and high-luminosity LHC: cross-section predictions and theoretical uncertainty projections

Convenors:
A. Calderon Tazon[1], J.M. Campbell[2], F. Caola[3,4], P. Francavilla[5,6], G. Marchiori[5]

Contributors:
K. Becker[7], C. Bertella[8], M. Bonvini[9], X. Chen[10], R. Frederix[11], S. Frixione[12], T. Gehrmann[10], E.W.N. Glover[4], Y. Haddad[13], V. Hirschi[14], A. Huss[15], S.P. Jones[15], A. Karlberg[10], M. Kerner[10], J. Lindert[4], G. Luisoni[16], S. Marzani[17,12], A. Massironi[15], B. Mistlberger[18], P.F. Monni[15], M. Moreno Llacer[15], A. Mueck[19], D. Pagani[11] C. Palmer[20], C. Pandini[15], L. Perrozzi[14], S. Pozzorini[10], E. Re[15,21], L. Reina[22], H.-S. Shao[23], L. Simon[19], B. Stieger[24], V. Theeuwes[25,26], F. Tramontano[27,28], M. Zaro[29]

[1]IFCA, Santander; [2]Fermilab; [3]U. Oxford; [4]Durham U., IPPP; [5]LPNHE, Paris; [6]INFN, Pisa; [7]U. Freiburg, Inst. Phys.; [8]CAS, Beijing; [9]INFN, Rome 1; [10]U. Zurich, Phys. Inst.; [11]Tech. U., Munich, Dept. Phys.; [12]INFN, Genoa; [13]Imperial Coll., London, Dept. Phys.; [14]ETH, Zurich, Dept. Phys.; [15]CERN, Geneva; [16]MPI Phys., Munich; [17]U. Genoa, Dept. Phys.; [18]MIT, Cambridge, CTP; [19]RWTH, Aachen, Phys. Inst.; [20]Princeton U.; [21]LAPTH, Annecy; [22]Florida State U., Tallahassee, Dept. Phys.; [23]LPTHE, Paris; [24]U. Nebraska, Lincoln, Dept. Phys. Astron.; [25]U. Gottingen, Inst. Theor. Phys.; [26]IPhT, Saclay; [27]U. Naples, Dept. Phys. Sci.; [28]INFN, Naples; [29]Nikhef, Amsterdam

Abstract

This note summarizes the state-of-the-art predictions for the cross sections expected for Higgs boson production in the 27 TeV proton-proton collisions of a high-energy LHC, including a full theoretical uncertainty analysis. It also provides projections for the progress that may be expected on the timescale of the high-luminosity LHC and an assessment of the main limiting factors to further reduction of the remaining theoretical uncertainties.

[1] *https://twiki.cern.ch/twiki/bin/view/LHCPhysics/LHCHXSWG*

Contents

1 Introduction

In this note, we present state-of-the-art theoretical predictions for Higgs boson production at the high-energy (HE) LHC (pp collisions at $\sqrt{s} = 27$ TeV), and their associated theoretical uncertainties. We also discuss projections of progress towards a reduction in theoretical uncertainties, on the timescale of the high-luminosity (HL) LHC (3 ab^{-1} of pp collisions at $\sqrt{s} = 14$ TeV). For all theoretical predictions reported in this note, we use a Higgs boson mass of $m_H = 125.09 \pm 0.5$ GeV, and set all other relevant parameters as in YR4 [1], with exceptions noted where they are important. The rest of this note is organised as follows. In Section 2 we present theoretical predictions for the Higgs production cross section at the HE-LHC, and compare them with predictions at the 13 TeV and 14 TeV LHC. Projections of theoretical uncertainties at the HL-LHC are discussed in Section 3. In Section 4 we present predictions for boosted Higgs production, both at the HL and at the HE LHC. Tables summarising a detailed study of the dependence of the gluon-fusion cross section on the mass of the Higgs boson are shown in Appendix A.

2 Cross sections for the HE-LHC

This section provides updated cross-sections for the LHC operating at energies of 13, 14 and 27 TeV. All predictions include the latest theoretical input and supersede the older results in YR4 [1].

2.1 Gluon fusion

In this section we document cross section predictions for a standard model Higgs boson produced through gluon fusion in 27 TeV pp collisions. To derive predictions we include contributions based on perturbative computations of scattering cross sections as studied in Ref. [2]. We include perturbative QCD corrections through N^{3}LO, electro-weak and approximated mixed QCD-electro-weak corrections as well as effects of finite quark masses. The only modification with respect to YR4 [1] is that we now include the exact N^{3}LO heavy top effective theory cross section of Ref. [3] instead of its previous approximation. The result of this modification is only a small change in the central values and uncertainties. To derive theoretical uncertainties we follow the prescriptions outlined in Ref. [2]. We use the following inputs:

$\mathrm{E_{CM}}$	27 TeV
$\mathrm{m_t(m_t)}$	162.7 GeV
$\mathrm{m_b(m_b)}$	4.18 GeV
$\mathrm{m_c}$(3 GeV)	0.986 GeV
$\alpha_S(m_Z)$	0.118
PDF	PDF4LHC15_nnlo_100 [4]

(1)

All quark masses are treated in the $\overline{\mathrm{MS}}$ scheme. To derive numerical predictions we use the program `iHixs` [5].

Sources of uncertainty for the inclusive Higgs boson production cross section have been assessed recently in refs. [1, 2, 6, 7], and we refer to reader to these references for a detailed discussion of the issue. Here we limit ourselves to summarise the main findings of those references. Several sources of theoretical uncertainties were identified.

- Missing higher order effects of QCD corrections beyond N^{3}LO (δ(scale)).
- Missing higher order effects of electro-weak and mixed QCD-electro-weak corrections at and beyond $\mathcal{O}(\alpha_S\alpha)$ (δ(EW)).
- Effects due to finite quark masses neglected in QCD corrections beyond NLO (δ(t,b,c) and $\delta(1/m_t)$).
- Mismatch in the perturbative order of the parton distribution functions evaluated at NNLO and the perturbative QCD cross sections evaluated at N^{3}LO (δ(PDF-TH)).

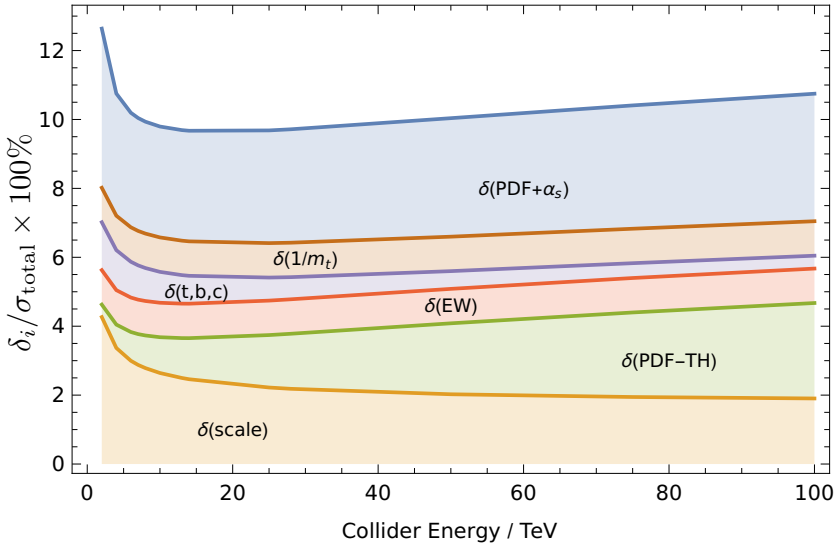

Fig. 1: The figure shows the linear sum of the different sources of relative uncertainties as a function of the collider energy. Each coloured band represents the size of one particular source of uncertainty as described in the text. The component $\delta(\text{PDF} + \alpha_S)$ corresponds to the uncertainties due to our imprecise knowledge of the strong coupling constant and of parton distribution functions combined in quadrature.

In the tables the linear sum of the effect of those uncertainties is referred to as $\delta(\text{theory})$. In addition, the imprecise knowledge of the parton distribution functions and of the strong coupling constant play a dominant role. The individual size of these contributions can be seen in fig. 1 as a function of the collider energy [5]. As can be easily inferred the relative importance of the different sources of uncertainty is impacted only mildly by changing the centre of mass energy from 13 TeV to 27 TeV. Inclusive cross sections for $m_H = 125.09$ GeV are given in Table 1. As noted above, the exact treatment of N^{3}LO QCD corrections results in a small shift in the cross-section at 13 TeV, relative to the YR4 resut, and a slight reduction in the overall theoretical uncertainty.

$\sqrt{s}$	σ	$\delta(\text{theory})$	$\delta(\text{PDF})$	$\delta(\alpha_s)$
13 TeV	48.61 pb	$^{+2.08\text{pb}}_{-3.15\text{pb}}$ $\binom{+4.27\%}{-6.49\%}$	$\pm 0.89\,\text{pb}\,(\pm 1.85\%)$	$^{+1.24\text{pb}}_{-1.26\text{pb}}$ $\binom{+2.59\%}{-2.62\%}$
14 TeV	54.72 pb	$^{+2.35\text{pb}}_{-3.54\text{pb}}$ $\binom{+4.28\%}{-6.46\%}$	$\pm 1.00\,\text{pb}\,(\pm 1.85\%)$	$^{+1.40\text{pb}}_{-1.41\text{pb}}$ $\binom{+2.60\%}{-2.62\%}$
27 TeV	146.65 pb	$^{+6.65\text{pb}}_{-9.44\text{pb}}$ $\binom{+4.53\%}{-6.43\%}$	$\pm 2.81\,\text{pb}\,(\pm 1.95\%)$	$^{+3.88\text{pb}}_{-3.82\text{pb}}$ $\binom{+2.69\%}{-2.64\%}$

Table 1: Gluon fusion Higgs boson production cross sections and uncertainties as a function of the pp collider energy.

The dependence of the inclusive gluon-fusion cross-section on the Higgs boson mass at $\sqrt{s} = 14$ and 27 TeV is detailed at the end of this note in Section A.

2.1.1 *Impact of threshold and high-energy corrections*

Recently, Ref. [8] has performed a study of the effects of simultaneous threshold and high-energy (small Bjorken x) resummations on the inclusive Higgs boson production cross section. In this brief section we summarise the main conclusions, while the numerical results will be discussed in the following section. For more details we refer the reader to Ref. [8]:

1. At different collider energies, it was found that the impact of threshold resummation amounts to about $+1\%$ on top of the N^{3}LO cross section [7]. The size of this effect is compatible with other estimates of the size of missing higher order corrections.
2. Conversely, the inclusion of small-x resummation was found to increase the cross section by about one percent at 13 TeV, and by about $3\% - 4\%$ at 27 TeV, with respect to the N^{3}LO prediction. The correction grows even larger at higher energies, reaching about $+10\%$ for a 100 TeV pp collider. The inclusion of high-energy resummation affects differently the perturbative coefficient functions and the parton densities.
   - The effect on the coefficient functions is very moderate, and remains below the 1% level for different collider energies. This indicates that the production of a Higgs boson at present and future colliders does not probe very small values of the momentum fraction at which the coefficient functions are evaluated. In turn, this implies that currently and at future colliders PDFs are probed at intermediate values of x.
   - The parton densities receive a large correction from small-x resummation. Its effect is twofold: on one hand, the *evolution* of the gluonic density is modified by the inclusion of small-x effects, and at average values of x probed in Higgs production this leads to a moderate effect on the parton densities at m_H (cf. Fig. 2.2 of Ref. [9]). On the other hand, the parton densities used in the double-resummed prediction of Ref. [8] (`NNPDF31sx_nnlonllx_as_0118` [9]) include small-x data from HERA, which Ref. [9] observes to require high-energy resummation for the fit to be robust. The fixed-order prediction of Ref. [8] instead uses a PDF set which fits the small-x HERA data without including high-energy resummation (`NNPDF31sx_nnlo_as_0118` [9]). This results in sizeable differences in the parton distribution functions and drives the large correction to the N^{3}LO total cross section observed in Ref. [8].

Summarising, the sizeable corrections to the N^{3}LO prediction due to high-energy resummation observed in Ref. [8] are, to a large extent, due to the need for high-energy resummation in the PDF fit which are necessary to get a reliable description of small-x HERA data. Performing a fit without high energy resummation results in considerable tension with respect to low-Q^2 HERA data. In order to corroborate these findings, and assess precisely the effect of high-energy resummation on parton distribution fits, it is important to make progresses in the theoretical knowledge of small-x dynamics. Furthermore, it would be desirable to include additional small-x collider data in the fits of parton distributions. We would like to encourage the PDF and theory community to further investigate these effects in view of future high energy colliders.

2.1.1.1 *Predictions for double-resummed cross section*

The setup is the same of the YR4 ($m_H = 125$ GeV, $m_t = 172.5$ GeV, $m_b = 4.92$ GeV, $m_c = 1.51$ GeV, $\alpha_s(m_Z^2) = 0.118$, $\mu_{\rm F} = \mu_{\rm R} = m_H/2$), with the only difference being that we do not use PDF4LHC but the `NNPDF31sx_nnlonllx_as_0118` set of Ref. [9]. Since these resummed PDFs are available for a single value of α_s, we could not compute the α_s uncertainty in our result. The results are collected in Tab. 2.

For each value of the collider energy, we give the full N^{3}LO+N^{3}LL+LLx cross section which includes top, bottom and charm contributions (as discussed in Ref. [10]) and EW corrections included

$\sqrt{s}$	$\sigma_{\text{N}^3\text{LO+N}^3\text{LL+LL}x}$	$= \sigma_t + \Delta\sigma_{bc} + \Delta\sigma_{\text{EW}}$	$\delta^{42\text{var}}_{\text{scale}}$	δ_{PDFs}	$\delta_{\text{subl.logs}}$	$\frac{\sigma_{\text{N}^3\text{LO+N}^3\text{LL+LL}x}}{\sigma_{\text{N}^3\text{LO}}}$
13 TeV	48.93 pb	$(49.26 - 2.66 + 2.33)$ pb	$^{+4.0}_{-3.8}\%$	$\pm 1.2\%$	$\pm 1.8\%$	1.020
14 TeV	55.22 pb	$(55.56 - 2.96 + 2.63)$ pb	$^{+4.0}_{-3.8}\%$	$\pm 1.1\%$	$\pm 1.9\%$	1.023
27 TeV	151.6 pb	$(151.6 - 7.2 + 7.2)$ pb	$^{+4.0}_{-4.0}\%$	$\pm 1.0\%$	$\pm 2.3\%$	1.046

Table 2: Values of the N^{3}LO+N^{3}LL+LLx gluon-fusion cross section for selected values of the pp collision energy and for a Higgs boson mass $m_{\text{H}} = 125$ GeV. We use the NNPDF31sx PDFs with $\alpha_s(m_Z^2) = 0.118$, $m_{\text{t}} = 173$ GeV, $m_{\text{b}} = 4.92$ GeV and $m_{\text{c}} = 1.51$ GeV.

in the complete factorization approach, i.e. as a $+5\%$ contribution. The breakdown of the individual terms contributing to the cross section (the main contribution assuming only top runs in the loop, the bottom+charm correction, and the EW correction) is presented in the third column. In the next columns, we present various sources of uncertainties, following Ref. [8]:

- Missing higher order uncertainty (scale uncertainty) $\delta^{42\text{var}}_{\text{scale}}$. It is the envelope of standard 7-point scale variations for each of the subleading variations of threshold resummed contributions, resulting in a total of 42 variations.
- PDF uncertainty δ_{PDFs}. This is the standard NNPDF Monte Carlo replica uncertainty, but it does not contain the α_s uncertainty, as previously discussed.
- Subleading small-x logarithms uncertainty $\delta_{\text{subl.logs}}$. This uncertainty is computed as described in Refs. [8, 10], and it likely overestimates the effect of subleading contributions in the coefficient functions. However, as argued in Refs. [8, 10], this uncertainty can be considered as an estimate of the uncertainty from subleading contributions in the PDFs. In this respect, this provides an alternative to the uncertainty from missing higher order PDFs adopted in YR4, which should thus not be included.

Additional uncertainties from missing $1/m_t^2$ effects, missing bottom+charm effects and subleading EW effects should be included according to the YR4 prescription. Since the N^{3}LO heavy-top result is matched to the exact small-x according to the construction of Ref. [10], the "truncation of the soft expansion" uncertainty discussed in YR4 should not be considered.

Finally, in the last column of the table we present the ratio of our resummed result with a purely fixed-order N^{3}LO cross section obtained with the same settings but using the NNLO PDFs `NNPDF31sx_nnlo_as_0118` of Ref. [9]. This is useful to understand how large the effect of resummation(s) in our prediction is. We see in particular that the effect (of small-x resummation) grows with the collider energy, reaching 4.6% at the HE-LHC. For any of the scales, approximately $+1\%$ of the effect of resummations is due to threshold resummation (in the coefficient functions), while the rest of the effect is due to small-x resummation, which mostly comes from the PDFs (see Ref. [8]) as discussed in the previous subsection.

2.2 Vector boson fusion

The vector-boson fusion (VBF) cross sections are computed with the same settings as in YR4 and reported in Tab. 3. The description of the setup can be found in the YR4 itself. For the 13, 14, and 27 TeV cross sections, the EW and photon cross sections have been computed using the `LUXqed_plus_PDF4LHC_nnlo_100` [11, 12] PDF set and hence the 13 and 14 TeV cross sections differ slightly from those reported in the YR4, where `NNPDF23_nlo_as_0118_qed` [13] was used instead. The QCD cross section was computed at NNLO with proVBFH [14, 15], while the EW and photon contributions have been computed at NLO with HAWK [16–18].

$\sqrt{s}$ [TeV]	σ^{VBF} [pb]	Δ_{scale} [%]	$\Delta_{\text{PDF}\oplus\alpha_s}$ [%]	$\sigma^{\text{DIS}}_{\text{NNLO}}$ [pb]	δ_{ELWK} [%]	σ_γ [pb]	$\sigma_{s\text{-ch}}$ [pb]
13	3.766	$^{+0.43}_{-0.33}$	± 2.1	3.939	-5.3	0.035	1.412
14	4.260	$^{+0.45}_{-0.34}$	± 2.1	4.460	-5.4	0.041	1.555
27	11.838	$^{+0.66}_{-0.36}$	± 2.1	12.483	-6.2	0.129	3.495

Table 3: VBF Higgs boson production cross-sections in pp collisions for center-of-mass energies up to 27 TeV and a Higgs boson mass $m_H = 125.09$ GeV. The s-channel cross-section is the contribution from Higgs-strahlung diagrams with hadronic weak-boson decay [1].

$\sqrt{s}$ [TeV]	$\sigma_{\text{NNLO QCD}\otimes\text{NLO EW}}$ [pb]	Δ_{scale} [%]	$\Delta_{\text{PDF}\oplus\alpha_s}$ [%]
13	1.358	$^{+0.51}_{-0.51}$	1.35
14	1.498	$^{+0.51}_{-0.51}$	1.35
27	3.397	$^{+0.29}_{-0.72}$	1.37

Table 4: Cross-section for the process $pp \to WH$. Both W^+ and W^- contributions are included. The photon contribution is not included. Results are given for a Higgs boson mass $m_{\text{H}} = 125.09$ GeV.

$\sqrt{s}$ [TeV]	$\sigma_{\text{NNLO QCD}\otimes\text{NLO EW}}$ [pb]	Δ_{scale} [%]	$\Delta_{\text{PDF}\oplus\alpha_s}$ [%]
13	0.831	$^{+0.74}_{-0.73}$	1.79
14	0.913	$^{+0.64}_{-0.76}$	1.78
27	1.995	$^{+0.43}_{-1.04}$	1.84

Table 5: Cross-section for the process $pp \to W^+H$. The photon contribution is not included. Results are given for a Higgs boson mass $m_{\text{H}} = 125.09$ GeV.

$\sqrt{s}$ [TeV]	$\sigma_{\text{NNLO QCD}\otimes\text{NLO EW}}$ [pb]	Δ_{scale} [%]	$\Delta_{\text{PDF}\oplus\alpha_s}$ [%]
13	0.527	$^{+0.59}_{-0.63}$	2.03
14	0.585	$^{+0.55}_{-0.68}$	1.98
27	1.402	$^{+0.36}_{-0.93}$	2.03

Table 6: Cross-section for the process $pp \to W^-H$. The photon contribution is not included. Results are given for a Higgs boson mass $m_{\text{H}} = 125.09$ GeV.

We note that the photon induced contribution is more reliably predicted here than was the case in the YR4 due to the LUXqed method. In particular the photon PDF should no longer be considered as a source of uncertainty as in eq. (I.5.7) in the YR4, as it is now constrained at the percent level. Quantitatively the photon induced contributions are reduced by about 30% compared to in the YR4.

The s-channel contributions at 13 and 14 TeV have on the other hand increased compared to the YR4 results. This is due to the updated PDF used for this prediction, i.e. `LUXqed_plus_PDF4LHC_nnlo_100` instead of `NNPDF23_nlo_as_0118_qed`. We also note that the relative size of the s-channel decreases as the collider energy increases - from 47% at 7 TeV to 30% at 27 TeV.

2.3 VH production

In Tabs. 4–13 we report the inclusive cross sections for associated production of a Higgs boson and a weak gauge boson $V = W, Z$, for pp collisions at 13, 14 and 27 TeV. The results have been obtained

$\sqrt{s}$ [TeV]	$\sigma_{\text{NNLO QCD}\otimes\text{NLO EW}}$ [pb]	Δ_{scale} [%]	$\Delta_{\text{PDF}\oplus\alpha_s}$ [%]	σ_γ
13	0.094	$^{+0.71}_{-0.70}$	1.72	$4.1\ 10^{-3}$
14	0.104	$^{+0.61}_{-0.73}$	1.70	$4.7\ 10^{-3}$
27	0.232	$^{+0.40}_{-0.97}$	1.72	$1.5\ 10^{-2}$

Table 7: Cross-section for the process $pp \to l^+\nu H$. The photon contribution is included, and also reported separately in the last column. Results are given for a Higgs boson mass $m_{\text{H}} = 125.09$ GeV.

$\sqrt{s}$ [TeV]	$\sigma_{\text{NNLO QCD}\otimes\text{NLO EW}}$ [pb]	Δ_{scale} [%]	$\Delta_{\text{PDF}\oplus\alpha_s}$ [%]	σ_γ
13	0.0598	$^{+0.57}_{-0.60}$	1.94	$2.6\ 10^{-3}$
14	0.0666	$^{+0.52}_{-0.64}$	1.89	$3.1\ 10^{-3}$
27	0.1628	$^{+0.34}_{-0.87}$	1.90	$1.1\ 10^{-2}$

Table 8: Cross-section for the process $pp \to l^-\bar{\nu}H$. The photon contribution is included, and also reported separately in the last column. Results are given for a Higgs boson mass $m_{\text{H}} = 125.09$ GeV.

$\sqrt{s}$ [TeV]	$\sigma_{\text{NNLO QCD}\otimes\text{NLO EW}}$ [pb]	Δ_{scale} [%]	$\Delta_{\text{PDF}\oplus\alpha_s}$ [%]
13	0.880	$^{+3.50}_{-2.68}$	1.65
14	0.981	$^{+3.61}_{-2.94}$	1.90
27	2.463	$^{+5.42}_{-4.00}$	2.24

Table 9: Cross-section for the process $pp \to ZH$. The predictions for the $gg \to ZH$ channel are computed at LO, rescaled by the NLO K-factor in the $m_{\text{t}} \to \infty$ limit, and supplemented by the NLL_{soft} resummation. The photon contribution is omitted. Results are given for a Higgs boson mass $m_{\text{H}} = 125.09$ GeV.

$\sqrt{s}$ [TeV]	$\sigma_{\text{NNLO QCD}\otimes\text{NLO EW}}$ [pb]	Δ_{scale} [%]	$\Delta_{\text{PDF}\oplus\alpha_s}$ [%]
13	0.758	$^{+0.49}_{-0.61}$	1.78
14	0.836	$^{+0.51}_{-0.62}$	1.82
27	1.937	$^{+0.56}_{-0.74}$	2.37

Table 10: Cross-section for the process $pp \to ZH$. The photon and $gg \to ZH$ contributions are omitted. Results are given for a Higgs boson mass $m_{\text{H}} = 125.09$ GeV.

$\sqrt{s}$ [TeV]	$\sigma_{\text{NNLO QCD}\otimes\text{NLO EW}}$ [pb]	Δ_{scale} [%]	$\Delta_{\text{PDF}\oplus\alpha_s}$ [%]
13	0.123	$^{+24.9}_{-18.8}$	4.37
14	0.145	$^{+24.3}_{-19.6}$	7.47
27	0.526	$^{+25.3}_{-18.5}$	5.85

Table 11: Cross-section for the process $gg \to ZH$. Predictions are computed at LO, rescaled by the NLO K-factor in the $m_{\text{t}} \to \infty$ limit, and supplemented by the NLL_{soft} resummation. Results are given for a Higgs boson mass $m_{\text{H}} = 125.09$ GeV.

$\sqrt{s}$ [TeV]	$\sigma_{\text{NNLO QCD}\otimes\text{NLO EW}}$ [pb]	Δ_{scale} [%]	$\Delta_{\text{PDF}\oplus\alpha_s}$ [%]	σ_γ
13	$2.97\ 10^{-2}$	$^{+3.49}_{-2.67}$	1.64	$1.4\ 10^{-4}$
14	$3.31\ 10^{-2}$	$^{+3.59}_{-2.92}$	1.89	$1.6\ 10^{-4}$
27	$8.32\ 10^{-2}$	$^{+5.39}_{-3.97}$	1.85	$5.4\ 10^{-4}$

Table 12: Cross-section for the process $pp \to l\bar{l}H$. The photon contribution is included, and reported separately in the last column. Results are given for a Higgs boson mass $m_{\text{H}} = 125.09$ GeV.

$\sqrt{s}$ [TeV]	$\sigma_{\text{NNLO QCD}\otimes\text{NLO EW}}$ [pb]	Δ_{scale} [%]	$\Delta_{\text{PDF}\oplus\alpha_s}$ [%]
13	0.177	$^{+3.50}_{-2.68}$	1.65
14	0.197	$^{+3.59}_{-2.92}$	1.89
27	0.496	$^{+5.41}_{-3.99}$	2.24

Table 13: Cross-section for the process $pp \to \nu\bar{\nu}H$. Results are given for a Higgs boson mass $m_{\text{H}} = 125.09$ GeV.

using HAWK, combining NNLO QCD and NLO EW corrections [18–22], by means of a multiplicative scheme, as described in the YR4 studies (eq. I.5.15 and I.5.16 of Ref. [1]). For ZH production, the loop-induced $gg \to ZH$ channel has been computed at NLO+NLL (using a Born-improved HEFT approach) [23, 24] and added linearly.

The contribution from photon-induced channels depends on the specific decay mode of the vector boson, and thus it has been removed from the total cross-sections, while it is instead included in the total result for the dedicated cross-sections where decay products are specified. In the latter cases, the individual photon-induced cross section is also separately reported.

The results at 27 and 14 TeV show a similar pattern of good perturbative convergence. There are two points that deserve some specific comment:

1. As can be evinced from the above tables, photon-induced contributions are relatively important in the $pp \to l^{\pm}\nu H$ case (where they amount to $\sim 4-7\%$ of the total cross section). For the $pp \to l\bar{l}H$ case instead, they contribute to only $\sim 4-7$ permille.
   We also notice that the relative weight of the photon-induced channel is computed more reliably than in the results previously obtained for the YR4 study: the changes in the values of σ_γ from the YR4 results (which also had large uncertainties) to those presented here are indeed non-negligible, and they are due to the fact that the photon PDF is now constrained significantly better, thanks to the LUXqed approach [11, 12]. We refer the reader to paragraph I.5.2.c of the YR4 for details on how this channel was treated previously. For the numbers in the new tables, the cross section for σ_γ was computed using the LUXqed_plus_PDF4LHC15_nnlo PDF set. For completeness, we also included an update for the 13 TeV cross sections using this PDF set.
2. As far as the loop-induced $gg \to ZH$ process is concerned, we remind that this channel starts contributing only at order α_S^2, hence it is part of the NNLO corrections to the $pp \to ZH$ cross section. Nevertheless, due to the gluonic luminosity, its relative size is important, especially at large center-of-mass energies. Due to the fact that it is a loop-induced channel, this contribution is known exactly (i.e. retaining finite values for the top mass) only at LO. However, because of its numerical size, and due to the fact that it contributes to the total cross section with a leading-order-like scale uncertainty, it is important to compute it at higher order. Exact NLO corrections to $gg \to ZH$ are not yet available. The numbers in the tables are obtained using a Born-improved HEFT approach, which essentially consists in computing the process at LO exactly, and rescaling it with the NLO/LO K-factor obtained in the $m_t \to \infty$ limit. NLL threshold effects have also been included. At order α_S^3 there are however many other gluon-gluon initiated subprocesses that

$m_{\rm H}$ [GeV]	$\sigma^{\rm NLO}_{\rm QCD+EW}$ [fb]	Scale [%]	α_s [%]	PDF [%]	PDF+α_s [%]
124.59	512.2	$^{+5.8}_{-9.2}$	2.0	3.0	3.6
125.09	506.5	$^{+5.8}_{-9.2}$	2.0	3.0	3.6
125.59	500.7	$^{+5.8}_{-9.2}$	2.0	3.0	3.6

Table 14: NLO QCD+EW cross sections for $t\bar{t}H$ production at the 13 TeV LHC, taken from Ref. [1].

$m_{\rm H}$ [GeV]	$\sigma^{\rm NLO}_{\rm QCD+EW}$ [fb]	Scale [%]	α_s [%]	PDF [%]	PDF+α_s [%]
124.59	619.3	$^{+6.1}_{-9.2}$	1.9	2.9	3.5
125.09	612.8	$^{+6.0}_{-9.2}$	1.9	2.9	3.5
125.59	605.6	$^{+6.1}_{-9.2}$	1.9	2.9	3.5

Table 15: NLO QCD+EW cross sections for $t\bar{t}H$ production at the 14 TeV LHC.

$m_{\rm H}$ [GeV]	$\sigma^{\rm NLO}_{\rm QCD+EW}$ [pb]	Scale [%]	α_s [%]	PDF [%]	PDF+α_s [%]
124.59	2.90	$^{+7.9}_{-9.0}$	1.8	2.1	2.8
125.09	2.86	$^{+7.8}_{-9.0}$	1.8	2.1	2.8
125.59	2.84	$^{+7.9}_{-9.0}$	1.8	2.1	2.8

Table 16: NLO QCD+EW cross sections for $t\bar{t}H$ production at a 27 TeV proton–proton collider.

$m_{\rm H}$ [GeV]	$\sigma_{t{\rm H}+\bar{t}{\rm H}}$ [fb]	Scale+FS [%]	α_s [%]	PDF [%]	PDF+α_s [%]	$\sigma_{t{\rm H}}$ [fb]	$\sigma_{\bar{t}{\rm H}}$ [fb]
124.59	74.52	$^{+6.6}_{-14.7}$	1.2	3.5	3.7	49.04	25.49
125.09	74.26	$^{+6.5}_{-14.7}$	1.2	3.5	3.7	48.89	25.40
125.59	74.09	$^{+6.5}_{-15.2}$	1.2	3.6	3.7	48.75	25.32

Table 17: NLO QCD cross sections for the $t-$channel tH and $\bar{t}H$ production at the 13 TeV LHC, taken from Ref. [1].

are not yet calculated. It is reasonable to expect that for VH the correction to the loop induced process will be the first at order α_S^3 to be evaluated in the near future, so that this contribution can provide an order of magnitude estimate of the remaining perturbative uncertainty coming from the missing higher orders.

2.4 $t\bar{t}H$ and tH

Cross sections for $t\bar{t}H$ and $tH + \bar{t}H$ production at $\sqrt{s} = 13,\ 14$ and 27 TeV are presented in Tables 14–16 and Tables 17–19 respectively. Results have been obtained using the same setup as in YR4, and considering three values for M_H, namely $M_H = 125.09 \pm 0.5$ GeV. The theoretical uncertainties from renormalization and factorization scale dependence, PDF, and α_s are calculated as explained in Sec. I.6.2 of YR4 [1], to which we refer for full details. $t\bar{t}H$ predictions include NLO QCD [25–31] and NLO QCD+EW corrections [30–32], while $tH + \bar{t}H$ predictions are accurate at NLO QCD only [33]. In both cases, `MadGraph5_aMC@NLO` [34, 35] has been employed for the computation of the cross sections. As expected, going to higher energies greatly enhances both $t\bar{t}H$ and $tH + \bar{t}H$ cross sections.

$m_{\rm H}$ [GeV]	$\sigma_{t{\rm H}+\bar{t}{\rm H}}$ [fb]	Scale+FS [%]	α_s [%]	PDF [%]	PDF+α_s [%]	$\sigma_{t{\rm H}}$ [fb]	$\sigma_{\bar{t}{\rm H}}$ [fb]
124.59	90.35	$^{+6.4}_{-14.6}$	1.2	3.4	3.6	59.15	31.21
125.09	90.12	$^{+6.4}_{-14.7}$	1.2	3.4	3.6	58.96	31.11
125.59	89.72	$^{+6.4}_{-14.8}$	1.2	3.4	3.6	58.70	31.02

Table 18: NLO QCD cross sections for the $t-$channel tH and $\bar{t}H$ production at the 14 TeV LHC.

$m_{\rm H}$ [GeV]	$\sigma_{t{\rm H}+\bar{t}{\rm H}}$ [fb]	Scale+FS [%]	α_s [%]	PDF [%]	PDF+α_s [%]	$\sigma_{t{\rm H}}$ [fb]	$\sigma_{\bar{t}{\rm H}}$ [fb]
124.59	419.0	$^{+5.0}_{-12.3}$	1.3	2.6	2.9	263.3	155.7
125.09	417.9	$^{+5.0}_{-12.5}$	1.3	2.6	2.9	262.8	155.1
125.59	416.4	$^{+5.0}_{-12.6}$	1.3	2.6	2.9	261.8	154.7

Table 19: NLO QCD cross sections for the $t-$channel tH and $\bar{t}H$ production at a 27 TeV proton–proton collider.

3 Projections of uncertainty reductions for the HL-LHC

This section discusses improvements to the theoretical predictions that may be possible on the timescale of the HL-LHC. Estimates of potential reductions in current theoretical uncertainties are made where possible and potential limiting factors identified.

3.1 Gluon fusion

Improving substantially on any of the current sources of uncertainty represents a major theoretical challenge that should be met in accordance with our ability to utilise said precision and with experimental capabilities. The computation of subleading mass and EW corrections is currently being addressed by several groups, and therefore it is likely to be achieved in the next decade. Although such computations will allow for a better control over some sources of uncertainty, their final impact on the full theoretical error is likely to be moderate as current estimates indicate. Another source of error that might improve in the forthcoming years is that related to the parton densities. In particular, the extraction of N^{3}LO PDFs would lead to the disappearance of the PDF-TH uncertainty. Similar considerations apply to the error on the strong coupling constant, that will be reduced due to more accurate extractions. Overall, the above progress would ultimately lead to a notable reduction of the uncertainties of Figure 1.

It is obvious that the future precision of experimental measurement of Higgs boson properties will challenge the theoretical community. Achieving a significant improvement of our current theoretical understanding of the Higgs boson and its interactions will inspire us to push the boundaries of our capabilities to predict and extract information. New ways of utilising quantum field theory in our endeavours have to be explored and our perturbative and non-perturbative understanding of hadron scattering processes has to evolve substantially. It is clear that this exciting task can only be mastered by a strong and active collider phenomenology community.

3.1.1 Impact of future precision of parton distribution function

It is a tantalising question to ask by how much one of the largest sources of uncertainty – the imprecise knowledge of PDFs – would be reduced if already all future LHC data were available. To this end a study was performed in ref. [36] that uses simulated future data with accordingly shrunken statistical uncertainties to constrain parton distribution functions. The authors used pseudo data corresponding to measurements of ATLAS, CMS and LHCb for key precision processes after 3ab^{-1} of integrated luminosity were collected at the High-Luminosity LHC at 14 TeV. They then performed a new fit according to the PDF4LHC15 framework [4] and studied the implications of their analysis. The resulting PDFs are readily available and can be used in order to estimate the impact of this future data on specific observables.

Three scenarios were considered in this study that assume that experimental systematic uncertainties will shrink at different levels relative to the 8 TeV run of the LHC. Scenario 1, scenario 2 and scenario 3 assume that the future systematic uncertainty will be equal, shrunk by a factor 0.7 or a factor of 0.4 w.r.t to the 8 TeV run respectively.

Evaluating the inclusive Higgs boson production cross section with this simulated PDFs results in the PDF uncertainties summarised in Tab. 20. Note, that the central values stay unchanged and all other uncertainties are not afflicted by the change of PDFs. Even the most pessimistic scenario leads to a

E_{CM}	Current	Scenario 1	Scenario 2	Scenario 3
13 TeV	$\pm 1.85\%$	$\pm 0.78\%$	$\pm 0.69\%$	$\pm 0.59\%$
14 TeV	$\pm 1.85\%$	$\pm 0.78\%$	$\pm 0.68\%$	$\pm 0.58\%$
27 TeV	$\pm 1.95\%$	$\pm 0.81\%$	$\pm 0.72\%$	$\pm 0.61\%$

Table 20: Uncertainty due to imprecise knowledge of PDFs estimated with current and simulated future PDFs for different scenarios and at different collider energies.

reduction of the PDF uncertainty by factor of two. However, these projections should be viewed only as a first estimate for the determination of PDFs from future measurements. Predicting the future development and correlation of systematic experimental uncertainties is non trivial and may differ strongly from observable to observable. PDF uncertainties may in the future also be adversely impacted by a more accurate treatment of theoretical uncertainties in the predictions of cross sections that serve as input for PDF extraction. Data incompatibilities may occur for various reasons. It is clear that an understanding of the structure of the proton at percent level accuracy is clearly a formidable task and rightly deserves significant research in the future.

3.2 Vector boson fusion

VBF Higgs boson production is currently known at a very high theoretical accuracy. In the structure-function approximation, the cross section has been computed fully inclusively at N^{3}LO accuracy in QCD. Fiducial calculations in the same approximation exist at NNLO accuracy in QCD. The only contribution which is currently unknown is the contribution from two-loop diagrams with gluon exchange between the two VBF quark lines. The conceptual difficulty is that it is a $2 \to 3$ process and that currently there are no methods available for evaluating two-loop diagrams with more than four external legs. It is realistic that such methods will become available before the HE-LHC is in operation. Beyond the VBF approximation, the full NLO corrections in both the strong and electroweak coupling have been computed for the Higgs plus 2 jets final state, and NLO QCD corrections to the Higgs plus 3 jet final state are available, as well [37]. The electroweak contributions are of the same order as, or in certain phase space regions even larger than, the NNLO QCD corrections. Taking all of this into account, it has been estimated that the VBF cross section under typical VBF cuts has an accuracy at the 1% level. In order to connect these calculations to experimental measurements one would ideally need merged 2- and 3-jet samples at the NLOPS level or even better a full NNLOPS generator for VBF. It is realistic that this will become available within the next few years and certainly before the HL/HE-LHC phases.

3.3 VH production

At the time of writing, the numbers shown in Section 2.3 are the best estimates available for the $pp \to VH$ contribution. As far as the ZH final state is concerned, due to the progress made in the last couple of years for the computation of top-mass effects at NLO in Higgs-boson pair production, it is foreseable that, in the forthcoming years (definitely in the timescale of HL/HE LHC), an exact NLO result (including

finite-m_t effects) will be available also for $gg \to ZH$. If one assumes that a pattern similar to what was found for di-higgs production [38, 39] also holds for $gg \to ZH$, one can expect that the total NLO/LO K-factor will be slightly smaller than in the HEFT limit (from 1.9–2.0 to $\sim$1.6) and the final scale uncertainty for the $gg \to ZH$ cross section will decrease from 18–25% to about 15%.[2]

All the above results have been obtained for a stable Higgs boson. For the Higgs boson decay to bottom quarks, it is known that higher-order corrections to the m_{bb} lineshape are relevant, as shown in Ref. [40] and also recently confirmed in Ref. [41]. Although explicit studies are not available, one can expect that effects similar to those observed at 13–14 TeV in the region $m_{bb} < m_H$ will persist also at higher energies.

The matching of fixed-order corrections to parton showers (PS) is available for the $pp \to VH$ signal processes, at NLO as well as at NNLO [42, 43]. As for Higgs decays to bottom quarks, a fixed-order study [41] suggests that higher-order corrections to the m_{bb} shape are not always very well modelled by a LO + parton shower treatment of the $H \to b\bar{b}$ decay. Event generators as the one developed in Ref. [43], and improvements thereof for the treatment of radiation off b-quarks [44], will allow one to assess this issue in the forthcoming years. A solid prediction of the $H \to b\bar{b}$ decay, also matched to parton-showers, can definitely be expected in the timescale of HL/HE LHC.

Furthermore, once the exact $gg \to ZH$ computation at NLO will be completed, a NLO matching to parton-shower will be straightforward to achieve, thereby improving on the currently available more advanced treatments, where a LO-merging of the exact matrix elements for $gg \to ZH$ and $gg \to ZH$+1-jet is performed.

Finally, as for the VH and VHJ event generators, recently there has been also the completion of the NLO EW corrections matched to the parton shower [45] showing once again the relevance of the EW corrections for the distributions for both the fixed order and the matched predictions.

3.4 $t\bar{t}H$ and tH

The cross sections for $t\bar{t}H$ and tH production are known at NLO accuracy in QCD [25, 27, 33] and, in the case of $t\bar{t}H$, NLO EW [30, 31] and NLO+NNLL [46, 47] corrections have also been calculated. The corresponding theoretical uncertainty is of the order of 10–15% and is mainly induced by the residual scale dependence and, to a lesser extent, by PDF uncertainties. A drastic improvement can only come from the calculation of the NNLO QCD corrections. Given the ongoing rapid progress in cross section calculations with NNLO accuracy in QCD, it is foreseeable that NNLO QCD corrections to $t\bar{t}H$ and tH will become available in the next decade. In this scenario it is reasonable to expect a factor-two improvement of the theoretical accuracy.

On the other hand, the extraction of the $t\bar{t}H$ signal is at the moment mainly limited by the theoretical uncertainties in the modelling of the background, mainly $t\bar{t}b\bar{b}$ and $t\bar{t}W$+jets, via Monte Carlo generators. The reliable assessment of the related uncertainties and their further reduction are the main goals of an ongoing campaign of theoretical studies within the HXSWG. On a time scale of 5–10 years such background uncertainties may be reduced by a factor two to three.

[2] We stress that these numbers have been obtained as a back-of-the-envelope estimate through a comparison with di-higgs production.

4 Higgs production at large transverse momentum

The HL and HE LHC upgrades would allow for in-depth analyses of the high-p_t tail of the Higgs boson transverse momentum distribution. This region is particularly interesting as it is very sensitive to BSM physics in the Higgs sector. For example, measurements in the boosted region would allow one to lift the degeneracy between ggH and ttH couplings, and in general probe the internal structure of the ggH interaction.

We first present results for the 13 TeV LHC. In Fig. 2(left) we show the cumulative Higgs transverse momentum distribution, defined as

$$\Sigma(p_t^H) = \int_{p_t^H}^{\infty} \frac{d\sigma}{dp_t},$$

for the main production channels. The ggF prediction is obtained by rescaling the exact NLO [48,

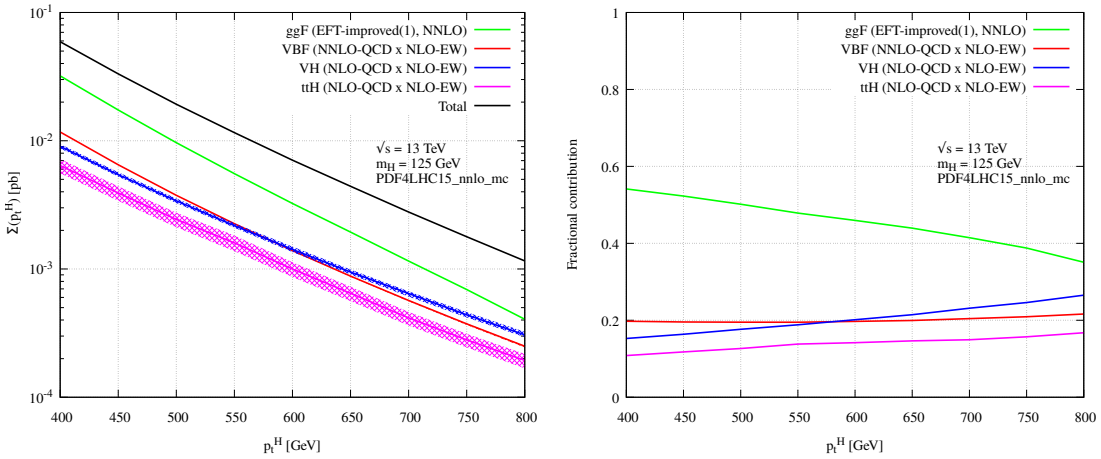

Fig. 2: Boosted Higgs prediction at the 13-TeV LHC. Left: cumulative transverse momentum distribution. Right: relative importance of different production mechanisms. See text for details.

49] with the NNLO $K-$factor in the $m_t \to \infty$ approximation [50–52], and it does not contain EW corrections. The VBF prediction includes NNLO QCD and NLO EW corrections, while the VH and $t\bar{t}H$ predictions include NLO QCD and EW corrections [14, 53–56]. For ggF, the factorization and renormalization scales are chosen to be $\mu_F^2 = \mu_R^2 = m_H^2 + p_{\perp,H}^2$. For VBF, we use $\mu_F^2 = \mu_R^2 = (m_H/2) \times \sqrt{(m_H/2)^2 + p_{\perp,H}^2}$, see [14]. For VH, we use $\mu_F^2 = \mu_R^2 = (p_V + p_H)^2$, while for $t\bar{t}H$ we use $\mu_F^2 = \mu_R^2 = (m_{\perp,t} + m_{\perp,\bar{t}} + m_{\perp,H})^2/4$.

In Fig. 2(right), we show the relative importance of the different production mechanisms.[3] As it is well known, at high p_t the ggF channel becomes somewhat less dominant. Still, radiative corrections strongly enhance this channel, which remains the dominant one in the TeV region. A very similar picture is expected for the HL-LHC.

Figs. 3 and 4 show similar predictions for the HE-LHC. In Fig. 3, all predictions are LO. At high p_t, the ggF channel become subdominant compared to the other ones. VBF becomes the dominant channel around $p_t \sim 1$ TeV, and VH around $p_t \sim 2$ TeV. In the TeV region, the $t\bar{t}H$ channel becomes larger than ggF.

[3] The small feature around $p_t \sim 750$ GeV in the ggF channel is due to lack of statistics in the theoretical simulation and it is not a genuine physical feature.

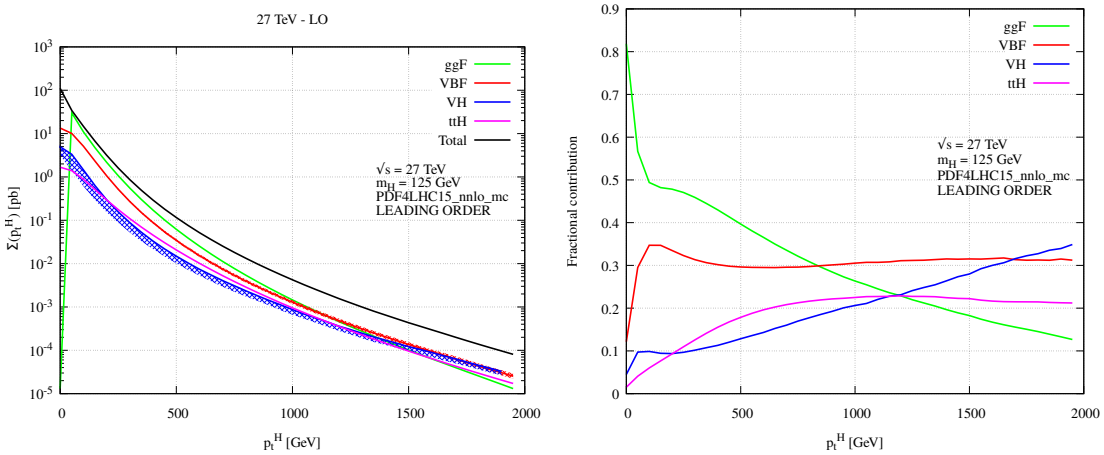

Fig. 3: LO boosted Higgs prediction at the 27-TeV LHC. Left: cumulative transverse momentum distribution. Right: relative importance of different production mechanisms. See text for details.

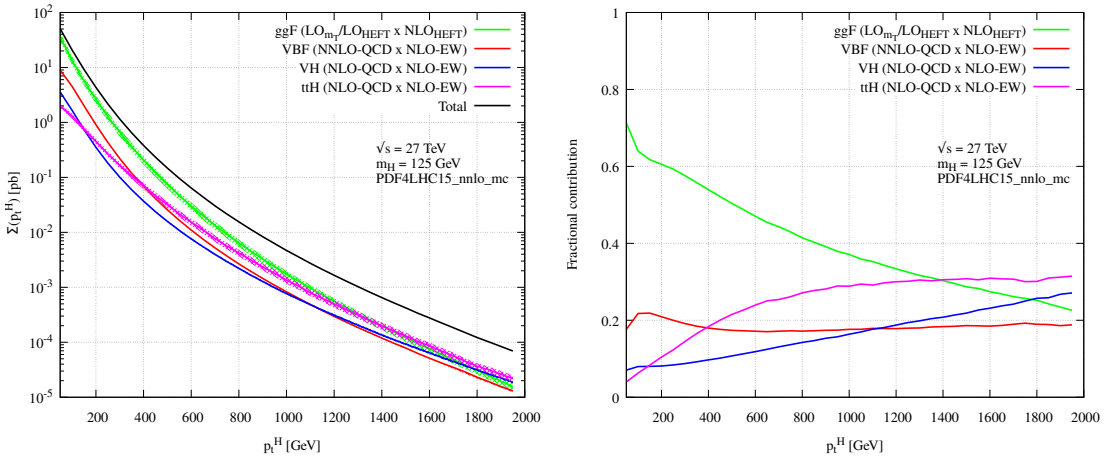

Fig. 4: Boosted Higgs prediction at the 27-TeV LHC, including radiative corrections. Left: cumulative transverse momentum distribution. Right: relative importance of different production mechanisms. See text for details.

This picture is however significantly altered by radiative correction, whose size and impact varies significantly between the different channels. This is shown in Fig. 4, where predictions include radiative corrections. More precisely, the VBF, VH and $t\bar{t}H$ predictions have the same accuracy as the ones in Fig. 2. The ggF prediction contains exact LO mass effects rescaled by the NLO $K-$factor in the m_t approximation. This is expected to provide an excellent approximation of the exact NLO result. Radiative corrections enhance the relative importance of the ggF and $t\bar{t}H$ channels, which still dominate over VBF well into the multi-TeV region. At large $p_t \sim 1.5$ TeV, the $t\bar{t}H$ channel becomes the dominant one.

Obtaining accurate and precise theoretical predictions in the boosted region is very challenging. Nevertheless, it is natural to expect progress on the timescale of the HL and HE LHC upgrades. This would allow for a proper scrutiny of the structure of Higgs interactions in the multi-TeV regime.

Appendices

A Dependence of gluon-fusion cross section at 14 and 27 TeV on m_H

The dependence of the inclusive gluon-fusion cross-section on the Higgs boson mass is shown in Tables A.1 and A.2, for pp collisions at $\sqrt{s} = 14$ and 27 TeV, respectively.

m_H [GeV]	Cross Section [pb]	+ δTh. [%]	- δTh. [%]	$\pm\delta$(PDF+α_S) [%]	$\pm\delta\alpha_S$ [%]	$\pm\delta$ PDF [%]
125.09	54.72	4.29	−6.46	3.20	2.61	1.85
124.59	55.10	4.29	−6.48	3.20	2.61	1.86
125.59	54.34	4.28	−6.45	3.20	2.61	1.85
120.00	58.85	4.37	−6.61	3.23	2.63	1.87
120.50	58.42	4.37	−6.60	3.22	2.63	1.87
121.00	58.00	4.36	−6.58	3.22	2.63	1.87
121.50	57.56	4.35	−6.57	3.22	2.62	1.86
122.00	57.15	4.34	−6.55	3.22	2.62	1.86
122.50	56.75	4.33	−6.54	3.21	2.62	1.86
123.00	56.35	4.32	−6.52	3.21	2.62	1.86
123.50	55.95	4.31	−6.51	3.21	2.61	1.86
124.00	55.56	4.30	−6.49	3.21	2.61	1.86
124.10	55.48	4.30	−6.49	3.20	2.61	1.86
124.20	55.41	4.30	−6.49	3.20	2.61	1.86
124.30	55.33	4.30	−6.49	3.20	2.61	1.86
124.40	55.25	4.30	−6.48	3.20	2.61	1.86
124.50	55.17	4.30	−6.48	3.20	2.61	1.86
124.60	55.10	4.29	−6.48	3.20	2.61	1.86
124.70	55.02	4.29	−6.47	3.20	2.61	1.86
124.80	54.94	4.29	−6.47	3.20	2.61	1.86
124.90	54.86	4.29	−6.47	3.20	2.61	1.86
125.00	54.79	4.29	−6.47	3.20	2.61	1.86
125.10	54.71	4.29	−6.46	3.20	2.61	1.85
125.20	54.64	4.28	−6.46	3.20	2.61	1.85
125.30	54.56	4.28	−6.46	3.20	2.61	1.85
125.40	54.48	4.28	−6.45	3.20	2.61	1.85
125.50	54.41	4.28	−6.45	3.20	2.61	1.85
125.60	54.33	4.28	−6.45	3.20	2.61	1.85
125.70	54.26	4.28	−6.44	3.20	2.61	1.85
125.80	54.18	4.27	−6.44	3.20	2.60	1.85
125.90	54.11	4.27	−6.44	3.20	2.60	1.85
126.00	54.03	4.27	−6.44	3.20	2.60	1.85
126.50	53.66	4.26	−6.42	3.19	2.60	1.85
127.00	53.29	4.25	−6.41	3.19	2.60	1.85
127.50	52.92	4.25	−6.40	3.19	2.60	1.85
128.00	52.56	4.24	−6.38	3.19	2.60	1.85
128.50	52.20	4.23	−6.37	3.18	2.59	1.85
129.00	51.85	4.22	−6.35	3.18	2.59	1.85
129.50	51.50	4.21	−6.34	3.18	2.59	1.84
130.00	51.15	4.20	−6.33	3.18	2.59	1.84

Table A.1: The gluon-fusion cross-section in pp collisions at $\sqrt{s} = 14$ TeV, for different values of the Higgs boson mass m_H.

m_H [GeV]	Cross Section [pb]	+ δTh. [%]	- δTh. [%]	$\pm\delta$(PDF+α_S) [%]	$\pm\delta\alpha_S$ [%]	$\pm\delta$ PDF [%]
125.09	146.65	4.53	−6.43	3.30	2.66	1.95
124.59	147.55	4.55	−6.45	3.30	2.67	1.95
125.59	145.75	4.52	−6.42	3.30	2.66	1.95
120.00	156.35	4.64	−6.60	3.33	2.69	1.97
120.50	155.36	4.63	−6.58	3.33	2.69	1.97
121.00	154.36	4.62	−6.56	3.33	2.69	1.97
121.50	153.38	4.61	−6.55	3.32	2.68	1.96
122.00	152.41	4.60	−6.54	3.32	2.68	1.96
122.50	151.45	4.59	−6.52	3.32	2.68	1.96
123.00	150.50	4.58	−6.50	3.31	2.68	1.96
123.50	149.56	4.57	−6.49	3.31	2.67	1.96
124.00	148.64	4.56	−6.47	3.31	2.67	1.95
124.10	148.45	4.56	−6.47	3.31	2.67	1.95
124.20	148.27	4.56	−6.46	3.31	2.67	1.95
124.30	148.08	4.55	−6.46	3.31	2.67	1.95
124.40	147.90	4.55	−6.46	3.31	2.67	1.95
124.50	147.72	4.55	−6.46	3.31	2.67	1.95
124.60	147.53	4.55	−6.45	3.30	2.67	1.95
124.70	147.35	4.54	−6.45	3.30	2.67	1.95
124.80	147.17	4.54	−6.44	3.30	2.67	1.95
124.90	146.99	4.54	−6.44	3.30	2.67	1.95
125.00	146.81	4.54	−6.44	3.30	2.67	1.95
125.10	146.63	4.53	−6.43	3.30	2.66	1.95
125.20	146.45	4.53	−6.43	3.30	2.66	1.95
125.30	146.27	4.53	−6.43	3.30	2.66	1.95
125.40	146.09	4.53	−6.42	3.30	2.66	1.95
125.50	145.91	4.52	−6.42	3.30	2.66	1.95
125.60	145.73	4.52	−6.42	3.30	2.66	1.95
125.70	145.55	4.52	−6.41	3.30	2.66	1.95
125.80	145.37	4.52	−6.41	3.30	2.66	1.95
125.90	145.20	4.52	−6.41	3.30	2.66	1.95
126.00	145.02	4.51	−6.40	3.30	2.66	1.95
126.50	144.14	4.50	−6.39	3.29	2.66	1.94
127.00	143.26	4.49	−6.37	3.29	2.66	1.94
127.50	142.40	4.48	−6.36	3.29	2.65	1.94
128.00	141.54	4.48	−6.34	3.28	2.65	1.94
128.50	140.69	4.47	−6.33	3.28	2.65	1.94
129.00	139.84	4.46	−6.31	3.28	2.65	1.93
129.50	139.00	4.46	−6.30	3.27	2.64	1.93
130.00	138.18	4.45	−6.29	3.27	2.64	1.93

Table A.2: The gluon-fusion cross-section in pp collisions at $\sqrt{s} = 27$ TeV, for different values of the Higgs boson mass m_H.

References

[1] D. de Florian et al. Handbook of LHC Higgs Cross Sections: 4. Deciphering the Nature of the Higgs Sector. 2016.

[2] Charalampos Anastasiou, Claude Duhr, Falko Dulat, Elisabetta Furlan, Thomas Gehrmann, Franz Herzog, Achilleas Lazopoulos, and Bernhard Mistlberger. High precision determination of the gluon fusion Higgs boson cross-section at the LHC. *JHEP*, 05:058, 2016.

[3] Bernhard Mistlberger. Higgs boson production at hadron colliders at N^3LO in QCD. *JHEP*, 05:028, 2018.

[4] Michiel Botje et al. The PDF4LHC Working Group Interim Recommendations. 2011.

[5] Falko Dulat, Achilleas Lazopoulos, and Bernhard Mistlberger. iHixs 2 — Inclusive Higgs cross sections. *Comput. Phys. Commun.*, 233:243–260, 2018.

[6] Robert V. Harlander, Stefan Liebler, and Hendrik Mantler. SusHi Bento: Beyond NNLO and the heavy-top limit. *Comput. Phys. Commun.*, 212:239–257, 2017.

[7] Marco Bonvini, Simone Marzani, Claudio Muselli, and Luca Rottoli. On the Higgs cross section at N^3LO+N^3LL and its uncertainty. *JHEP*, 08:105, 2016.

[8] Marco Bonvini and Simone Marzani. Double resummation for Higgs production. *Phys. Rev. Lett.*, 120(20):202003, 2018.

[9] Richard D. Ball, Valerio Bertone, Marco Bonvini, Simone Marzani, Juan Rojo, and Luca Rottoli. Parton distributions with small-x resummation: evidence for BFKL dynamics in HERA data. *Eur. Phys. J.*, C78(4):321, 2018.

[10] Marco Bonvini. Small-x phenomenology at the LHC and beyond: HELL 3.0 and the case of the Higgs cross section. *Eur. Phys. J.*, C78(10):834, 2018.

[11] Aneesh Manohar, Paolo Nason, Gavin P. Salam, and Giulia Zanderighi. How bright is the proton? A precise determination of the photon parton distribution function. *Phys. Rev. Lett.*, 117(24):242002, 2016.

[12] Aneesh V. Manohar, Paolo Nason, Gavin P. Salam, and Giulia Zanderighi. The Photon Content of the Proton. *JHEP*, 12:046, 2017.

[13] Richard D. Ball, Valerio Bertone, Stefano Carrazza, Luigi Del Debbio, Stefano Forte, Alberto Guffanti, Nathan P. Hartland, and Juan Rojo. Parton distributions with QED corrections. *Nucl. Phys.*, B877:290–320, 2013.

[14] Matteo Cacciari, Frederic A. Dreyer, Alexander Karlberg, Gavin P. Salam, and Giulia Zanderighi. Fully Differential Vector-Boson-Fusion Higgs Production at Next-to-Next-to-Leading Order. *Phys. Rev. Lett.*, 115(8):082002, 2015. [Erratum: Phys. Rev. Lett.120,no.13,139901(2018)].

[15] Frederic A. Dreyer and Alexander Karlberg. Vector-Boson Fusion Higgs Production at Three Loops in QCD. *Phys. Rev. Lett.*, 117(7):072001, 2016.

[16] M. Ciccolini, Ansgar Denner, and S. Dittmaier. Strong and electroweak corrections to the production of Higgs + 2jets via weak interactions at the LHC. *Phys. Rev. Lett.*, 99:161803, 2007.

[17] Mariano Ciccolini, Ansgar Denner, and Stefan Dittmaier. Electroweak and QCD corrections to Higgs production via vector-boson fusion at the LHC. *Phys. Rev.*, D77:013002, 2008.

[18] Ansgar Denner, Stefan Dittmaier, Stefan Kallweit, and Alexander Mueck. HAWK 2.0: A Monte Carlo program for Higgs production in vector-boson fusion and Higgs strahlung at hadron colliders. *Comput. Phys. Commun.*, 195:161–171, 2015.

[19] Robert V. Harlander, Jonas Klappert, Stefan Liebler, and Lukas Simon. vh@nnlo-v2: New physics in Higgs Strahlung. *JHEP*, 05:089, 2018.

[20] Ansgar Denner, Stefan Dittmaier, Stefan Kallweit, and Alexander Muck. Electroweak corrections to Higgs-strahlung off W/Z bosons at the Tevatron and the LHC with HAWK. *JHEP*, 03:075, 2012.

[21] Oliver Brein, Abdelhak Djouadi, and Robert Harlander. NNLO QCD corrections to the Higgs-

strahlung processes at hadron colliders. *Phys. Lett.*, B579:149–156, 2004.

[22] M. L. Ciccolini, S. Dittmaier, and M. Kramer. Electroweak radiative corrections to associated WH and ZH production at hadron colliders. *Phys. Rev.*, D68:073003, 2003.

[23] Lukas Altenkamp, Stefan Dittmaier, Robert V. Harlander, Heidi Rzehak, and Tom J. E. Zirke. Gluon-induced Higgs-strahlung at next-to-leading order QCD. *JHEP*, 02:078, 2013.

[24] Robert V. Harlander, Anna Kulesza, Vincent Theeuwes, and Tom Zirke. Soft gluon resummation for gluon-induced Higgs Strahlung. *JHEP*, 11:082, 2014.

[25] W. Beenakker, S. Dittmaier, M. Kramer, B. Plumper, M. Spira, and P. M. Zerwas. Higgs radiation off top quarks at the Tevatron and the LHC. *Phys. Rev. Lett.*, 87:201805, 2001.

[26] W. Beenakker, S. Dittmaier, M. Kramer, B. Plumper, M. Spira, and P. M. Zerwas. NLO QCD corrections to t anti-t H production in hadron collisions. *Nucl. Phys.*, B653:151–203, 2003.

[27] L. Reina and S. Dawson. Next-to-leading order results for t anti-t h production at the Tevatron. *Phys. Rev. Lett.*, 87:201804, 2001.

[28] S. Dawson, L. H. Orr, L. Reina, and D. Wackeroth. Associated top quark Higgs boson production at the LHC. *Phys. Rev.*, D67:071503, 2003.

[29] S. Dawson, C. Jackson, L. H. Orr, L. Reina, and D. Wackeroth. Associated Higgs production with top quarks at the large hadron collider: NLO QCD corrections. *Phys. Rev.*, D68:034022, 2003.

[30] Y. Zhang, W.-G. Ma, R.-Y. Zhang, C. Chen, and L. Guo. QCD NLO and EW NLO corrections to $t\bar{t}H$ production with top quark decays at hadron collider. *Phys. Lett.*, B738:1–5, 2014.

[31] S. Frixione, V. Hirschi, D. Pagani, H. S. Shao, and M. Zaro. Electroweak and QCD corrections to top-pair hadroproduction in association with heavy bosons. *JHEP*, 06:184, 2015.

[32] S. Frixione, V. Hirschi, D. Pagani, H. S. Shao, and M. Zaro. Weak corrections to Higgs hadroproduction in association with a top-quark pair. *JHEP*, 09:065, 2014.

[33] Federico Demartin, Fabio Maltoni, Kentarou Mawatari, and Marco Zaro. Higgs production in association with a single top quark at the LHC. *Eur. Phys. J.*, C75(6):267, 2015.

[34] J. Alwall, R. Frederix, S. Frixione, V. Hirschi, F. Maltoni, O. Mattelaer, H. S. Shao, T. Stelzer, P. Torrielli, and M. Zaro. The automated computation of tree-level and next-to-leading order differential cross sections, and their matching to parton shower simulations. *JHEP*, 07:079, 2014.

[35] R. Frederix, S. Frixione, V. Hirschi, D. Pagani, H. S. Shao, and M. Zaro. The automation of next-to-leading order electroweak calculations. *JHEP*, 07:185, 2018.

[36] Rabah Abdul Khalek, Shaun Bailey, Jun Gao, Lucian Harland-Lang, and Juan Rojo. Towards Ultimate Parton Distributions at the High-Luminosity LHC. *Eur. Phys. J.*, C78(11):962, 2018.

[37] Francisco Campanario, Terrance M. Figy, Simon Plätzer, and Malin Sjödahl. Electroweak Higgs Boson Plus Three Jet Production at Next-to-Leading-Order QCD. *Phys. Rev. Lett.*, 111(21):211802, 2013.

[38] S. Borowka, N. Greiner, G. Heinrich, S. P. Jones, M. Kerner, J. Schlenk, and T. Zirke. Full top quark mass dependence in Higgs boson pair production at NLO. *JHEP*, 10:107, 2016.

[39] Julien Baglio, Francisco Campanario, Seraina Glaus, Margarete Muehlleitner, Michael Spira, and Juraj Streicher. Gluon fusion into Higgs pairs at NLO QCD and the top mass scheme. *Eur. Phys. J.*, C79(6):459, 2019.

[40] Giancarlo Ferrera, Gabor Somogyi, and Francesco Tramontano. Associated production of a Higgs boson decaying into bottom quarks at the LHC in full NNLO QCD. *Phys. Lett.*, B780:346–351, 2018.

[41] Fabrizio Caola, Gionata Luisoni, Kirill Melnikov, and Raoul Roentsch. NNLO QCD corrections to associated WH production and $H \to b\bar{b}$ decay. *Phys. Rev.*, D97(7):074022, 2018.

[42] William Astill, Wojciech Bizon, Emanuele Re, and Giulia Zanderighi. NNLOPS accurate associated HW production. *JHEP*, 06:154, 2016.

[43] William Astill, Wojciech Bizon, Emanuele Re, and Giulia Zanderighi. NNLOPS accurate associated HZ production with NLO decay $\mathrm{H} \to b\bar{b}$. *Submitted to: JHEP*, 2018.

[44] L. Buonocore, P. Nason, and F. Tramontano. Heavy quark radiation in NLO+PS POWHEG generators. *Eur. Phys. J.*, C78(2):151, 2018.

[45] Federico Granata, Jonas M. Lindert, Carlo Oleari, and Stefano Pozzorini. NLO QCD+EW predictions for HV and HV +jet production including parton-shower effects. *JHEP*, 09:012, 2017.

[46] Alessandro Broggio, Andrea Ferroglia, Ben D. Pecjak, and Li Lin Yang. NNLL resummation for the associated production of a top pair and a Higgs boson at the LHC. *JHEP*, 02:126, 2017.

[47] Anna Kulesza, Leszek Motyka, Tomasz Stebel, and Vincent Theeuwes. Associated $t\bar{t}H$ production at the LHC: Theoretical predictions at NLO+NNLL accuracy. *Phys. Rev.*, D97(11):114007, 2018.

[48] R. Keith Ellis, I. Hinchliffe, M. Soldate, and J. J. van der Bij. Higgs Decay to tau+ tau-: A Possible Signature of Intermediate Mass Higgs Bosons at the SSC. *Nucl. Phys.*, B297:221–243, 1988.

[49] U. Baur and E. W. Nigel Glover. Higgs Boson Production at Large Transverse Momentum in Hadronic Collisions. *Nucl. Phys.*, B339:38–66, 1990.

[50] Radja Boughezal, Fabrizio Caola, Kirill Melnikov, Frank Petriello, and Markus Schulze. Higgs boson production in association with a jet at next-to-next-to-leading order. *Phys. Rev. Lett.*, 115(8):082003, 2015.

[51] X. Chen, T. Gehrmann, E. W. N. Glover, and M. Jaquier. Precise QCD predictions for the production of Higgs + jet final states. *Phys. Lett.*, B740:147–150, 2015.

[52] John M. Campbell, R. Keith Ellis, and Satyajit Seth. H+1 jet production revisited. 2019.

[53] T. Gleisberg, Stefan. Hoeche, F. Krauss, M. Schonherr, S. Schumann, F. Siegert, and J. Winter. Event generation with SHERPA 1.1. *JHEP*, 02:007, 2009.

[54] Fabio Cascioli, Philipp Maierhofer, and Stefano Pozzorini. Scattering Amplitudes with Open Loops. *Phys. Rev. Lett.*, 108:111601, 2012.

[55] Stefan Kallweit, Jonas M. Lindert, Philipp Maierhoefer, Stefano Pozzorini, and Marek Schoenherr. NLO electroweak automation and precise predictions for W+multijet production at the LHC. *JHEP*, 04:012, 2015.

[56] Gionata Luisoni, Paolo Nason, Carlo Oleari, and Francesco Tramontano. $HW^{\pm}$/HZ + 0 and 1 jet at NLO with the POWHEG BOX interfaced to GoSam and their merging within MiNLO. *JHEP*, 10:083, 2013.